Search for Binary Kuiper Belt Objects using Images from the Deep Ecliptic Survey and Magellan Telescopes

by

Sarah J. Eddy

Bachelor of Civil Engineering
The Catholic University of America, 2001

SUBMITTED TO THE DEPARTMENT OF EARTH, ATMOSPHERIC, AND PLANETARY SCIENCES IN PARTIAL FULFILLMENT OF THE REQUIREMENTS FOR THE DEGREE OF

MASTER OF SCIENCE IN GEOSYSTEMS
AT THE
MASSACHUSETTS INSTITUTE OF TECHNOLOGY

JUNE 2002

© Sarah J. Eddy 2002. All rights reserved.

The author hereby grants to MIT permission to reproduce and to distribute publicly paper and electronic copies of this thesis document in whole or in part.

Author.....
Department of Earth, Atmospheric, and Planetary Sciences
May 03, 2002

Certified by.....
James L. Elliot
Thesis Supervisor

Accepted by.....
Ronald G. Prinn
Head, Department of Earth, Atmospheric and Planetary Sciences

MASSACHUSETTS INSTITUTE OF TECHNOLOGY
JUL 19 2002
LIBRARIES
LINDGREN

Search for Binary Kuiper Belt Objects using Images from the Deep Ecliptic Survey and Magellan Telescopes

by
Sarah J. Eddy

Abstract

A method is developed for examining image frames containing Kuiper Belt objects and classifying those KBOs as binary candidate / not binary candidate. This method uses an elliptical point-spread function fitting technique, relying on the fact that a binary KBO system will appear in a telescope image as an elongated source, with more or less elongation depending on the separation distance and the relative intensity of the two components.

Mosaic images for forty-five Kuiper Belt objects from the Deep Ecliptic Survey were tested. Of these, four were binary candidates, twelve others were possible candidates, twenty-one were circular within detection limits, and seven lacked the consistent set of field stars necessary for determination.

Observations were planned for the nights of April 8-11, 2002 with the Magellan I telescope. However, due to unfavorable observing conditions during the three nights of the run, no good images of the ten candidate binaries and possible candidates visible at the time were able to be taken.

This methodology of image analysis should continue to be applied to new KBO images, to identify additional binary candidates. Imaging of the candidates selected through this thesis work will be attempted during future Magellan observing runs, particularly in June 2002.

Thesis Supervisor: James L. Elliot

Acknowledgements

Although the title page has my name on it, it is not the result of my work alone. Several people have contributed in various ways of their time to make this thesis a reality. I would like to thank the following individuals specifically for their valuable contributions:

First of all, *Jim Elliot*, my thesis supervisor, for his guidance, insightful suggestions, and confidence in my work throughout this project, without which I would by no means be finished, and for his autograph on the front cover of this thesis document endorsing this work and consenting to my graduation.

Susan Kern, for helping me get started on the project, teaching me everything I know about finding and cross-referencing DES images, and answering my many questions, and for being such a great friend.

Kelly Clancy, for going to Chile in my stead, even though the telescope time got rained out, and for beta-testing this method of fitting on a Magellan image frame.

Dale Morgan and *Daniel Burns*, my program advisors, for keeping me on track concerning the various deadlines.

The other members of the Geosystems group: *Jennifer Alltop, Bill Boos, Lisa Lassner,* and *Heather Hooper,* for their camaraderie and for their helpful comments and feedback throughout the year.

My parents, for their constant support, love, and encouragement, for listening when I was under stress and just needed to talk, and most especially for raising me to become the person I am now.

And finally, *the Lord*, who sustains me with his love and his truth, for the grace he gives me to follow where he leads.

Table of Contents

List of Tables

List of Figures

Chapter 1. Introduction

1.1 The Kuiper Belt

The Kuiper Belt is a region of the outer solar system beyond the orbit of Neptune, from 35 AU to at least 50 AU in extent. It contains the planetesimals known as Kuiper Belt objects (KBOs).

The existence of such a belt was first theorized by Kenneth Edgeworth (1943), and, after him, by Gerard Kuiper (1951). For this reason, the region is sometimes called the Edgeworth-Kuiper Belt.

Study of detected Kuiper Belt objects, on the other hand, is less than a decade old. The first known KBO was discovered in 1992 (Jewitt & Luu 1993), after years of fruitless searching by a number of astronomers. Since then, the rate of discovery has increased greatly. The orbits of approximately 600 Kuiper Belt objects are currently known with enough accuracy to be given provisional designations by the Minor Planet Center.

With the discovery of a large number of minor bodies in trans-Neptunian orbits in the past decade, our view of the outer solar system has been dramatically changed. The Kuiper Belt is a repository of the presumably most primitive material (least thermally processed by solar heating or UV bombardment) in the solar system (Trujillo, Jewitt & Luu 2001). As such, the information it provides is of great importance to our understanding of the origin and evolution of the outer solar system. Characterization of KBOs may provide insight into the physical and chemical processes predominant in the primitive solar nebula, as well as information on how our sun and solar system currently appear and may have appeared in the past, as viewed from a distance.

1.2 Surveys

"Pencil beam" surveying work is one method in use for detecting Kuiper Belt objects. Using the 3.6-m Canada-France-Hawaii Telescope and 8-m Very Large Telescope, these observations concentrate on a single field per night to obtain the maximum depth possible (Chiang & Brown 1999).

Wide-field CCD surveying is an alternate method of KBO discovery that attempts to observe large portions of the sky. Wide-field CCD surveys in the published literature include Sheppard et al. (2000), Larsen et al. (2001), Trujillo, Jewitt & Luu (2001), and Ferrin et al. (2001).

The survey of particular interest to this thesis is the Deep Ecliptic Survey (DES) for Kuiper Belt Objects and Centaurs. The DES is an ongoing wide-field survey being carried out by a Lowell-MIT-LBTO-Berkeley-University of Pennsylvania team, using the Mosaic cameras on the 4-m Mayall and Blanco telescopes at Kitt Peak National Observatory and Cerro Tololo Inter-American Observatory (Elliot et al. 2000; Millis et al. 2002). Because of the large area surveyed and the sensitivity of the Mosaic camera, the DES is acquiring a statistically large sample of KBOs. The average discovery rate is 15-20 objects per clear observing night, and their goal is to discover 500 objects in three years.

1.3 Dynamical KBO Classification

Kuiper Belt objects can be classified into three relatively distinct categories according to their orbital dynamics: classical, resonant, and scattered-disk objects.

1. Classical KBOs are so called because their semimajor axes, eccentricities and inclinations place them in the region originally expected to house the Kuiper Belt. Nearly circular, their orbits have semimajor axes greater than 40 AU. They have presumably undergone the least dynamical modification by either Neptune or some other source of dynamical excitation, and represent the leftover planetesimal disk.

2. Resonant KBOs include the Pluto-Charon system and all other objects orbiting the sun in mean motion resonances with Neptune. The *Plutinos* are trapped in the 3:2 resonance at 39 AU, while other KBOs inhabit the 2:1 resonance at approximately 48 AU.

3. There is no firm definition given for the scattered-disk objects. In general, they have highly eccentric and inclined orbits, much greater than those in the classical belt, and are taken here to include those KBOs classified as neither classical nor resonant.

The majority of discovered KBOs reside in the classical belt. Approximately one-third are in mean motion resonances with Neptune, and the remaining few are scattered objects (Brown, 2001).

1.4 Size Distribution and Radial Extent

Population estimates of the Kuiper Belt are based on sampling of the ecliptic by surveys such as those mentioned in the previous section. These samples suggest that more than 10^5 bodies with diameters greater than 100 kilometers inhabit the region of distances 30 to 50 AU (Jewitt, Luu, & Trujillo 1998), and that they have a combined mass on the order of 0.1 Earth masses (Jewitt et al. 1996; Jewitt et al. 1998). Classical Kuiper Belt objects have inclinations within about 15 degrees of the ecliptic, though KBOs with inclinations as high as 38 degrees have been discovered. The belt inclination distribution, best fit by two Gaussian curves rather than one, suggests that at least two classes of objects with different dynamical histories exist (Brown 2001).

The classical KBOs follow a differential power law size distribution with index $q \approx 4$ (Gladman et al. 2001; Luu & Jewitt 1998; Kenyon & Windhorst 2001). If there is a maximum KBO diameter, it must be greater than 1000km (Trujillo et al. 2001). KBOs with diameter greater than 50km have not had their size distribution modified by collisional processes (Davis & Farinella 1997), so for these objects, the distribution must be a result of accretion.

The number of large KBOs is of primary interest because it is a direct measurement of the accretion process and timescales in the outer solar system (Trujillo et al. 2001). The total mass of the present Kuiper Belt is 100 to 1000 times less than the amount calculated to have been

there in the beginning, by extrapolation either from the solid mass density of the giant planets or from the mass necessary for accretion of 100-km bodies during the lifetime of the solar system (Stern & Colwell 1997b).

The size distribution of KBOs appears to steep ($q \geq 4$) down to the 50-km diameter level, which is the modelled cutoff point between accretional and collisional processes; given this distribution, accretion must have proceeded for approximately 10Myr before the excitation of the inner Kuiper Belt (Gladman et al. 2001). The correction for the falloff of KBO density as a function of ecliptic latitude is uncertain (Elliot et al. 2000).

Very few low-eccentricity KBOs with semimajor axes greater than 48 AU have been discovered. According to some analyses, surveys should have detected such objects if they exist; this nondetection indicates the possible presence of an outer edge to the belt (Dones 1997; Jewitt et al. 1998; Allen et al. 2001; Trujillo et al. 2001). However, if the luminosity follows a steeper radial distribution, this nondetection outside 50 AU may not be significant (Gladman et al 1998, Chiang & Brown 1999). One possibility is that the disk outside 48 AU is dynamically very cold, and that this is what prevents detection so far (Hahn 2000). On the other hand, a robust estimation of the true radial distribution of KBOs from the apparent distribution, when applied to each of the three KBO groups, verified the pronounced drop in numbers at 47 ± 1 AU (Trujillo & Brown 2001).

1.5 Color

Much still needs to be learned about the physical properties of KBOs. The median R-magnitude is around 23, although there are several objects more than ten times brighter. The basis for size determinations of nearly all KBOs is that their optical properties are similar to cometary nuclei: the typical albedo is assumed to be 0.04 (Jewitt & Luu 2000). This is a natural assumption, since the majority of the short-period comets originate in the Kuiper Belt (Fernandez 1980; Duncan et al 1988). However, the surfaces of some KBOs and Centaurs are very red (Barucci et al 2001; Jewitt & Luu 2001), redder than cometary nuclei, possibly due to processing of the surface materials by cosmic ray bombardment over time (Wilson, Sagan & Thompson 1994, Cruikshank et al 1998). The ultrared matter must therefore be destroyed or removed during an evolutionary transition from KBO to short-period comet. One possible explanation involves resurfacing by sublimation, which occurs rapidly once the object enters the water sublimation zone (6 AU) (Jewitt 2002). Also, laboratory experiments on sublimating ice / refractory particles show color variations (Stephens & Gustalson 1991) that may match observed states.

There is also a large diversity in colors and spectra among the Kuiper Belt objects themselves (Green et al 1997). In fact, the most striking physical feature of KBOs is their large diversity of color, which ranges from nearly neutral to some of the reddest objects in the solar system (Jewitt & Luu 1998, Tegler & Romanishin 2000). This could be a result of collisional resurfacing processes (Luu & Jewitt 1996), or of an intrinsic difference in composition. KBOs can be strongly volatile depleted bodies, with outgassing of internal volatiles responsible for some of the observed spectral variation (De Sanctis, Capria, & Coradini 2001). The visible colors appear unrelated to infrared spectral properties, as KBOs may be differ greatly in the former and appear similar in the latter, or vice versa (Brown, Blake, & Kessler 2000).

The existence of a bimodal color distribution (Tegler & Romanishin 1998) is controversial (Barucci et al 2000; Davies et al. 2000; Hainaut & Delsanti 2001, Delsanti et al. 2001). If there is a bimodal color distribution, collisional resurfacing could not be the cause because it would produce intermediate colors as well.

The colors of the classical KBOs may have a correlation to their inclinations (Tegler & Romanishin 2000; Trujillo & Brown 2002). There is no such correlation with the Plutinos (resonant KBOs), and no significant correlation between color and any other orbital parameter. An inclination correlation could be expected if the KBOs are made up of different sub-populatons that have different primordial colors (Trujillo & Brown 2002).

Other dynamical groupings into sub-populations have also been proposed, consistent with the color bimodality. These include separation into large and small components of the classical KBOs (Levison & Stern 2001) and high inclination / low inclination orbits of the classical KBOs (Brown 2001).

1.6 Physical Processes

The inner part of the Kuiper Belt is the most probable source of the short-period comets, due to the gravitational perturbations of their orbits by the passages of Neptune and Uranus. In fact, it is likely that these and similar perturbations have shaped its current structure, and that the Kuiper Belt has evolved through collisions (Farinella & Davis 1996).

In the classical belt, the relative encounter speeds of KBOs are so large that accretion at this point is impossible: velocities after impact are much greater than the escape velocities. The classical belt is beyond the limits of scattering action by the giant planets on their current orbits (Gladman 2001).

Particular regions may be cleared out by gravitational erosion over the lifetime of the solar system, such as the gap between 40 and 42 AU (Duncan, Levison & Budd 1995). However, this cannot account for the mass loss in the belt by itself, unless the KBO population has also been perturbed by a strong force that excited most of the mass to dynamically unstable orbits. Some event(s) after the accretional stage of formation must have produced the observed orbital structure: the structure requires some additional process more complicated than accretion and erosion through collisions.

There are several proposed models, each of which explains some but not all of the observed structure. For example, angular momentum conservation implies that Neptune and Uranus migrated outward during the elimination of interplanetary planetesimals; KBOs on circular orbits would be trapped in Neptune's mean motion resonances as they were swept outward (Malhotra 1995). This model was extended by Hahn & Malhotra (1999) and Ida et al (2000a), who calculated trapping rates for the different resonances. The mechanism of resonance sweeping, however, does not significantly deplete Kuiper Belt mass.

Another scenario is that giant-planet embryos or cores, forming simultaneously with the giant

planet cores, were then scattered into orbits such that they passed repeatedly through the Kuiper Belt before being ejected from the solar system (Morbidelli & Valsecchi 1997; Petit, Morbidelli, & Valsecchi 1999; Levison, Lissauer & Duncan 1998). The resultant structure would be dependent on the orbital history of these bodies. It would be very effective for dynamically exciting the belt, as well as depleting it of mass, but it also would leave very few objects in the 3:2 resonance with Neptune.

Passing stars could also potentially excite the Kuiper Belt. Perihelion passages of one or several stars around 100-200 AU can produce eccentricity and inclination perturbations comparable to those observed beyond 42 AU (Ida et al 2000b). Resonance sweeping could still occur within 40 AU, although the problem of mass depletion in the resonance-swept areas (30-50 AU) remains. In this case, the excited region would not have an outer radial limit.

Secular resonance sweeping provides a fourth possible mechanism, modeled with idealized assumptions by Hahn & Ward (2002). A secular resonance is a point where the precession of the KBO matches an eigenfrequency of the solar system and can drive the object into a highly eccentric or inclined orbit. As the solar nebula gas is dispersed, these sources of dynamical excitation would sweep through the solar system and through the Kuiper Belt (Nagasawa et al, 2000).

Discrimination between these models and their variations seem to require a detailed knowledge of the orbits of a large number of KBOs, and especially those with large (>50 AU) heliocentric distances to determine if there is a dynamically cold disk at these far distances or not (Gladman 2001).

1.7 KBO Binaries

Kuiper Belt Object	**IAUC #**	**Discovery Separation**	**Delta Magnitude**	**Discovery Method**
Pluto-Charon	3241	0".9	2-3	US Naval Obs. 155-cm astrometric reflector
1998 WW31	7610	1".2	0.4	CFHT
2001 QT297	7733	0".6	0.55	Magellan
2001 QW322	7749	4"	0.	CFHT
1999 TC36	7787	0".37	2.2	HST
1998 SM165	7807	0".2	1.9	HST
1997 CQ29	7824	0".17	not given	HST
2000 CF105	7857	0".78	0.9	HST

Table 1.1 Published binary KBO discoveries and the telescopes used.

The first and best-known binary Kuiper Belt Object is the Pluto-Charon system. For several years, it was also the only known such binary. Then, in the spring of 2000, Veillet et al. discovered a second binary, 1998 WW31 (IAUC 7610). Yet another binary KBO was discovered with the MagIC camera on Magellan, by Dave Osip in October of 2001 (IAUC 7733). Each of the latter two binary systems was originally detected as single KBOs by the Deep Ecliptic Survey and not recognized as binary in its discovery data.

In the last few months, several other KBOs were determined to be binary. Table 1.1 above summarizes these findings.

It appears likely, then, that binaries are ubiquitous in the Kuiper Belt. Knowledge of more binaries, their existence, their numbers, and their properties, will provide insight into the mechanisms of their formation and the formation of the outer solar system.

In this thesis I present a method for examining KBO images taken with the Mosaic camera to determine whether or not it is a binary candidate, and apply it to 45 Kuiper Belt objects detected through the Deep Ecliptic Survey (Millis et al. 2002).

Chapter 2. A Brief Review of Binary Objects

2.1 Basics

A binary object is a special case in the class of satellite bodies where the masses of the two objects are such that their center of mass lies outside either body. Each companion orbits around the center of mass of the system. In this thesis, the term binary is used loosely, since it is unknown whether or not these KBO systems fit the rigorous definition.

For small, planetesimal-sized bodies in our solar system, the bodies traverse a heliocentric orbit in addition to their mutual revolution.

Figure 3.1 Illustration of a binary orbit outside 1 AU. Two times during its heliocentric orbit (points A below), the binary components will undergo mutual occultations and eclipses visible from Earth.

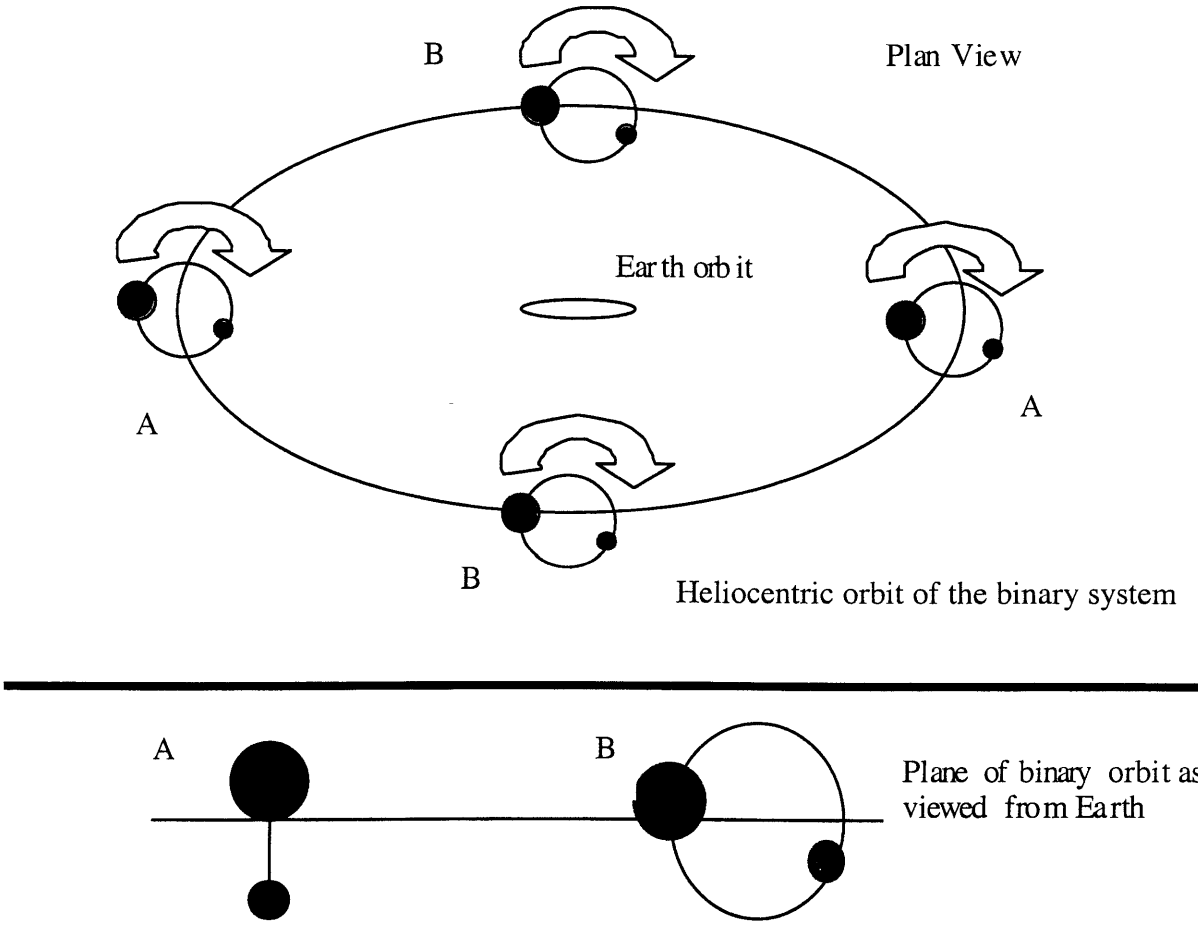

Plan view of the binary system at the two extremes in its (not necessarily circular) orbit. At points A in the top panel, the system is seen "edge-on" from Earth, while at points B it is "face-on".

All binary objects revolve around each other in a particular orbital plane. Since KBO binaries travel a heliocentric orbit, the Earth intersects the binary orbital plane twice during the period of solar revolution. When this occurs, the two bodies undergo a series of occultations and eclipses

visible from the Earth, whose heliocentric orbit is much shorter than that of the KBO system. This is illustrated in Figure 3.1.

Mutual events provide a framework from which one can determine an accurate diameter for each component: as one of the companions is occulted, its light curve drops. Precise measurement of the light curve for the duration of the occultation, combined with knowledge of the mutual orbit and thus the relative velocities of the components, will yield an accurate value for the diameter of the eclipsing body (e.g., Binzel & Hubbard 1998).

2.2 Formation Processes

In the Kuiper Belt, binary formation has only been explored with respect to the Pluto-Charon system. However, there are several dynamical processes in our solar system capable of producing binary systems (see Brown 2002):

1. Rotational fission. It is theoretically possible for a binary system to be formed from a single body by fission due to overspinning. Mutual gravitation and the strength of the material simply does not provide enough cohesive force to keep the bound components from literally flying apart. The cause of such overspinning is unknown, but may require close planetary interactions not operative in the Belt.

2. Impact formation / Fragmentation from a larger body. A scenario of catastrophic impact such as that proposed for the formation of the Earth-Moon system could cause the formation of other binary systems. An impactor colliding obliquely with a large object could break it into fragments that fly apart but remain gravitationally bound, and accrete to form a satellite, generating a binary.

3. Three-body gravitational capture. Orbital capture of an object requires energy dissipation. If a satellite is not already present, a three-body interaction will result in one body carrying off a large amount of energy if the remaining two bodies are to be left in bound orbits. A large number density of objects is required for this mechanism to be operative.

4. Impact formation and impact evolution. It is possible for a system to undergo multiple collisions; in this scenario, the initial formation of the binary could take place through the methods outlined above. Subsequent impacts into one or both members of the system would then bring about evolution of the binary orbit, with large expected eccentricities of the system as a result.

The Kuiper Belt objects 1998 WW31 and 2001 QT297 have binary components of similar brightness (Veillet 2001; Elliot 2001). An analysis of possible mechanisms of formation for these two binaries based on their orbital constraints (Brown 2002) concludes that the most probable scenario is catastrophic impact followed by collisional modification of the subsequent orbits. No single-event process appears capable of explaining the observed binaries' characteristics: Both rotational fission and catastrophic impact followed by tidal evolution would require a much smaller total angular momentum than is present in these systems. Fragmentation of a large parent object is unlikely given that model simulations produce comparable orbits for

mass ratios of less than 0.05. The probability of intact capture, assuming a satellite is not present to begin with, is exceedingly small even for lower KBO velocities and higher densities.

The probability of two or more collisions in the *present* Kuiper Belt is low (Durda & Stern 2000). In the more massive, dynamically unexcited early Kuiper Belt, collisions would have been much more frequent, though more apt to accretion than to binary formation. Therefore, the best time for binary formation would be during the transition from a high density of low-velocity bodies to the sparser high-velocity population that is the present day belt (Brown 2002).

2.3 Significance and Information

Observation of a binary Kuiper Belt Object allows establishment of its orbit, from which the separation distance and the system mass can be determined. Densities and albedos are extremely important properties, needed in order to fully understand KBO composition. They are fundamental for our understanding of the history and workings of the outer solar system.

For other solar system bodies, accurate masses have in general been determined by the deflection of satellites during fly-by missions; in the Kuiper Belt, an analogous determination is currently possible *only* by observation of binary systems.

Knowledge of the orbits of binary KBOs will provide statistical information on collisions and other processes that form binaries. It will allow determination of the separation distance and of the system mass. The relative magnitudes and colors of the binary companions are indicative of whether the objects are of similar or different materials and histories.

All binaries found eventually undergo mutual events, from which the diameter of each component can be determined precisely. The basic idea is that the relative velocity of the binary components seen from Earth can be calculated from knowledge of the orbit. As one component is occulted or eclipsed by the other, its light will diminish and then reappear; the ratio of the velocity to the length of time the lightcurve is affected is proportional to the size of the occulting body.

Precise densities and albedos can be calculated from the diameters, under the reasonable first-order assumption that the two components have similar compositional properties:

$$\rho = \frac{M_{system}}{V_{system}} = \frac{M_{system}}{\frac{4}{3}\pi\left(R_1^3 + R_2^3\right)} \qquad (1)$$

$$L_{reflected} = \pi A * F_o\left(\frac{r_o}{r_{KBO}}\right)^2 * \left(R_1^2 + R_2^2\right), \qquad (2)$$

where A is albedo, r_o and r_{KBO} are heliocentric distances, R_1 and R_2 are the radii of the components, and F_o is the solar flux at radius r_o. The second equation is for the simplest case in

which both bodies have the same albedo and are fully sunlit, with the sunlit area visible from Earth.

The determination of the mass and mean bulk density of KBOs provides a more accurate estimation of the total mass of the small bodies of the outer solar system. It will also undoubtedly yield better information concerning the origin and evolution of the short-period comets.

Chapter 3. Binary KBO Detection

The search for and characterization of binary systems among Kuiper Belt objects is particularly significant because of the information they provide regarding Kuiper Belt composition and evolution. The detection and observation of satellites of small bodies orbiting the Sun in the outer solar system—of KBO binaries, that is—is extremely important if one means to determine the orbit and masses of the components in such binary systems.

From their mutual orbit, system masses can be determined. For systems with observable eclipses and occultations, densities and albedos—of particular importance in determining KBO composition—can also be established.

The majority of discovered binary KBOs to date have been found as a result of deep field, high resolution images. Optical surveys may detect binaries with greater separation than the angular resolution limits of the surveys' techniques. The initial detection of new KBOs, on the other hand, is much more efficient with wide field-of-view cameras that can sample a greater portion of the sky in a given timeframe.

A brute force method of binary detection would be to simply attempt observation of all discovered KBOs with high resolution telescopes. Although this is indeed a possibility, and certainly a systematic one, it would require a great amount of telescope time: more telescope time, perhaps, than is necessary or prudent.

This thesis attempts to bridge the gap between surveying for new Kuiper Belt objects and searching for binaries among those already established. Analysis of the images taken with a wide field of view camera can be used to determine those KBOs that are likely binary candidates. Higher resolution images of these, fewer in number, binary KBO candidates can be taken with a higher expectation of detection success.

Of course, binary detections from this type of work will represent a lower limit on the total number or percentage of such systems, due to constraints in the luminosity and in the image frames themselves: each frame captures only one point in time of any particular orbit. The apparent separation distance between components varies depending on the relative position in orbit as viewed from Earth. Therefore, depending on the viewing angle at the time of observation, the components may be too close to be resolved. Tightly bound binaries may also be overlooked. Even so, statistical constraints—lower limits—may be placed on binary numbers and distribution within the KBO population.

Chapter 4. System Overview

The purpose of this research is to find additional binary Kuiper Belt objects. This is accomplished by undertaking a systematic search of the Mosaic images of KBOs already discovered through the Deep Ecliptic Survey (DES). The method of this search is one of image analysis, that is, the determination of the elongation of a KBO image after correcting for possible distorting factors in its image frame. Objects determined to be binary candidates are then to be observed using the higher-resolution Magellan telescopes, with a goal of increasing the signal-to-noise ratio at least five times that of the DES results, to verify or reject their status as candidate binary KBOs.

I examine archival images from the DES to search for candidate binary systems among the discovered Kuiper Belt Objects. Two of these, 1998 WW31 and 2001 QT297, are already known to be binary. However, they were not reported as binaries by their original discoverers; their duplicity was noted rather later, by visual inspection of higher resolution observations. The median seeing of the DES Mosaic data is about 1.3 arcsec, although images as good as 0.8 arcsec have been achieved. The binary nature of 2001 QT297, with components separated by 0.6 arcsec, was discovered with Magellan data in 0.4 arcsec seeing. Therefore, the higher resolution and good seeing of the Magellan telescopes may resolve other binaries hidden in the DES data more clearly.

Chapter 5. Development of Fitting Technique

This method and fitting technique was developed using the discovery frame of 2001 QT297, a known binary KBO, as a pilot case. The driving mechanism of this method is the determination of evidence of elongation in the image, after eliminating any source of ellipticity other than that caused by the duality of the source. Figure 6.1 illustrates the procedure described in this chapter, with a block diagram.

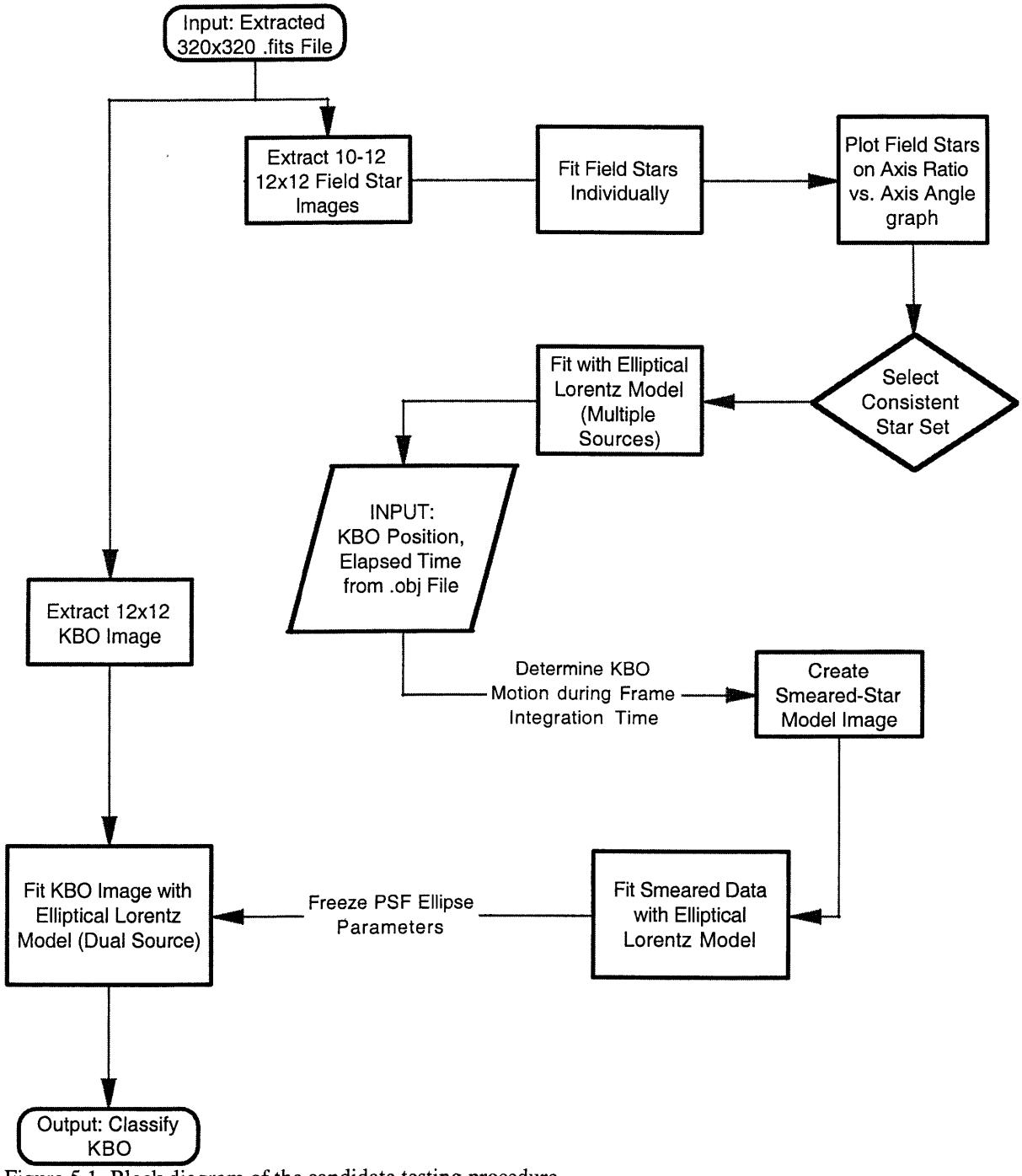

Figure 5.1 Block diagram of the candidate testing procedure.

5.1 Consistent Reference Star Set

After locating the DES file of the particular Mosaic frame containing the KBO image of interest, I extract a working frame (320x320 pixels, or approximately 168 arcsec each direction) from the 1024x2048-pixel binned original image size, centered on the KBO. This extraction greatly reduces the quantity of extraneous data with which I need deal.

From the working frame, approximately a dozen field stars are selected for individual analysis. The purpose of this preliminary "reference" fitting is the selection of a self-consistent star set by which to compare the KBO image. The elimination of galaxies from this set is important.

Around each of these stars, a box of 12x12 pixels comprises the data set for ellipse fitting. Here and throughout this thesis, "fitting" will refer to a least squares solution to the data points using an elliptical Lorentz point-spread function (Bosh et al. 1992). Four parameters define the fit of the ellipse (Elliot et al. 1989b):

1. The *axis ratio* α is the ratio of the minor axis to the major axis, always between 0 and 1.
2. The *axis angle* θ is the angle from the horizontal, East through North, of the major axis. This angle does not correspond directly to a physical quantity but depends on the orientation of the particular image frame.

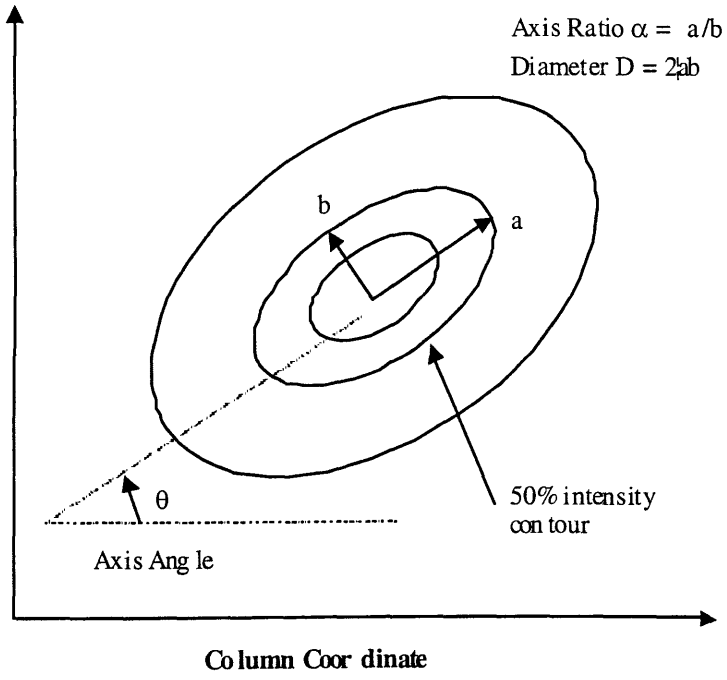

Figure 5.2 Illustration of the ellipse parameters used for least-squares fitting.

3. The *diameter D* is a measure of the size of the star in pixels, the mean image diameter between the half-peak-intensity points.

4. The *shape index p* is an parameter dictating the shape of the ellipse profile, that is, the luminosity as a function of position in the ellipse (Bosh et al. 1992):

$$Intensity(r) = \frac{1}{1 + \left(r / r_{1/2} \right)^{p}} \qquad (3)$$

where $r_{1/2}$ is the distance to the 50% intensity contour.

The field stars are then plotted on a graph of axis ratio versus axis angle, such as the one in Figure 6.2. From this plot, a self-consistent group (within error) of stars is chosen. This consistent star set is then fitted as a group, in order to determine the "average field star" ellipse parameters. These ellipse parameters provide the baseline against which any ellipticity in the KBO image may be measured.

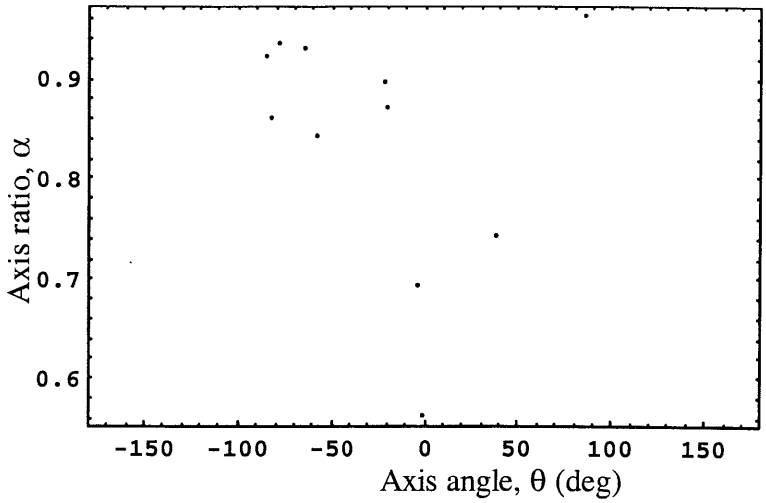

Figure 5.3. A dozen field stars from the DES frame 000731.096 are plotted according to their axis ratio and axis angle. The 320x320 extraction box was centered around 2001 QT297.

In this case, the seven stars loosely clustered near the top left would be taken as the consistent star set. The "star" with axis ratio less than 0.6 had a very patterned residual, and was probably a galaxy: even if it matched the others, it would not be used.

I then take the specified "average ellipse parameters" and use them to create a synthetic model of the average field star by assigning it a peak intensity of 1 with no background noise, a position centered in the box, and the ellipse parameters as stated.

5.2 Accounting for KBO Motion

One more intermediate, compensatory step remains. The integration time for the Mosaic frames is either 240 or 300 seconds, depending on the observing run. During this time, the location of the KBO is not fixed but is moving with some particular speed and direction. The row and column rates of motion were determined from KBO position on two captures of the same field during an observing run, using the following equations:

$$\dot{x} = \frac{(x_2 - x_1 - \Delta x_{12})}{\Delta t} \qquad (4)$$

$$\dot{y} = \frac{(y_2 - y_1 - \Delta y_{12})}{\Delta t} \tag{5}$$

where the positions are measured in pixels; x_1 and x_2 are the column positions (and y_1, y_2 the row) on the first and second frames taken of that field during the run, respectively; Δx_{12} and Δy_{12} are the horizontal and vertical offsets between the two frames; and Δt is the time elapsed time in hours between the two observations. The rate of motion measured in arcsec can be found by multiplying by the plate scale of the telescope. For Mosaic images, this scale is 0.526 arcsec per pixel; these have been binned (2x2) from the full resolution of the detector.

The synthetic star model was smeared according to the motion of the KBO, by summing eleven images evenly spaced along the path of motion:

$$P_i = \{0.,1.,\frac{i}{11} * \frac{\dot{y}}{T}, \frac{i}{11} * \frac{\dot{x}}{T}, D, \rho, \theta, \alpha\} \tag{6}$$

$$Model = \frac{1}{11} \sum_{i=-5}^{5} Ellipse(P_i) \tag{7}$$

where P_i is a list containing the background noise, the peak ratio, the center position in rows and columns, and the averaged field star ellipse parameters.

The synthetic smeared-star model was then fit with the elliptical Lorentz point-spread function. Note that the ellipse parameters to which the smeared-star model converge take into account effects both (1) from an unknown point-spread function affecting the original Mosaic frame as a whole and (2) from the motion of the KBO. Any further ellipticity in the image of the KBO, excepting noise, should depend only on whether or not a double source is present. The extent to which noise can cause ellipticity is indicated by the formal errors from the image fit.

5.3 Testing the KBO

Finally, the KBO image itself is fit, with an explicit specification in the model parameters for a double source. Three parameters and their standard errors determined the quality of the dual-source fit: the peak ratio, the row offset, and the column offset. The peak ratio is the ratio of the peak light intensity of the companion or fainter "secondary" component to the peak intensity of the brighter "primary" component. The row and column offsets are given in image pixels, and are a measure of the separation distance of the secondary component to the primary in arc-seconds. If both offsets converged to zero, the dual-source fit was said to collapse into a single source. In this case, the KBO effectively acts as a point source within detection limits.

5.4 Method Robustness

In order to determine how robust the fitting method is, testing was performed on the pilot image, the discovery frame of 2001 QT297, a known binary. To determine dependence on the initial parameter values, several selections of the initial parameter values were made, and the KBO

image fitted to convergence with each selection. The offset ranged from a quarter pixel to several pixels in each direction, and the peak ratio was varied between zero and unity.

In all cases, the elliptical fit converged to the same point in the parameter-space, as is shown in Table 5.1, below. Therefore I conclude that the method is fairly robust, and does not depend on previous knowledge of the separation or peak ratio in order to result in a convergent and precise fit. Table 5.2 shows a comparison of the difference in brightness and in position of the binary components as determined from fitting of the discovery Mosaic image frame and from subsequent Magellan observations.

Test Run	Peak $Ratio_0$	Row $Offset_0$	Column $Offset_0$	Peak $Ratio_F$	Row $Offset_F$ (pixels)	Column $Offset_F$ (pixels)
1	0.5	-0.5	1.0	0.67 ± 0.17	-1.67 ± 0.20	1.01 ± 0.20
2	0.5	0.5	-1.0	1.49 ± 0.38	1.66 ± 0.20	-1.01 ± 0.20
3	0.1	-3.0	3.0	0.67 ± 0.17	-1.67 ± 0.20	1.00 ± 0.20
4	0.5	-0.25	0.5	0.67 ± 0.17	-1.67 ± 0.20	1.01 ± 0.20
5	0.5	-1.0	2.0	0.67 ± 0.17	-1.66 ± 0.20	1.01 ± 0.20
6	0.7	-0.1	0.2	0.67 ± 0.18	-1.66 ± 0.19	1.01 ± 0.19
7	1.0	-0.05	0.05	0.67 ± 0.17	-1.66 ± 0.20	1.01 ± 0.19
8	2.0	-0.5	1.0	0.67 ± 0.17	-1.66 ± 0.20	1.01 ± 0.20

Table 5.1. The converged fit values for a variety of initial parameter values, using the DES image frame 000731.077. For test run 2, the components' positions and ratio were switched, and the model settled in to the reversed position with a correspondingly reversed peak ratio. (That is, 1 / 0.67 = 1.49.)

Data	Date of image frame	Delta Magnitude	Separation (arcsec)
IAUC 7733, 7765 Magellan	11 October, 2001	0.70 ± 0.20	0.61 ± 0.01
Mosaic image fitting technique	31 July, 2000	0.2 ± 0.1	1.0 ± 0.1

Table 5.2 Comparison of Mosaic fit results to Magellan observations.

Chapter 6. Application of the Method

6.1 KBO Image Selection

Sixty-nine Mosaic frames of forty-five Kuiper Belt Objects were tested using the method described above. The candidates were prioritized according to the following criteria:

- The KBO must have been discovered or imaged through the DES before or during February, 2002;
- The KBO must be visible during the 2002 Spring semester at Magellan;
- A brighter KBO should be given higher priority than a fainter KBO.

All KBOs with R-magnitudes brighter than 22.3 (where the result errors began to consistently saturate the signal) and satisfying the first two criteria were tested for candidacy.

6.2 Method Results

Several candidate binary KBO systems were discovered. The method results for selected objects are shown in Table 7.1, and a complete list may be found in Appendix B. Horizontal divisions group paired image frames, or multiple images taken of the same field during a particular observing run. When a second frame taken during the same observing run was tested, the results were checked against the first frame's parameters for consistency.

Each frame was classified as one of four categories according to its fitting results: Candidate, Possible, Circular, and No Conclusion.

1. Candidate: A KBO is classified as a candidate binary object if its peak ratio is significantly (at least one standard deviation) greater than zero in both of two paired frames, and has a definitive offset. "Definitive" refers qualitatively to the relative magnitude of the offset errors.

2. Possible: A KBO may be classified as a possible candidate if the fit results indicate a definite offset with a small nonzero (less than 0.2) peak ratio.

3. Circular: This definition applies if the standard error in the parameters is greater than the parameter values themselves. A KBO is also classified as circular if its peak ratio is zero within error even if there is a definitive row / column offset—but if the peak ratio could also be unity within error, it may be classified as possible. Finally, if the dual-source fit does not converge or the peak ratio becomes negative, it is also designated as circular within detection limits.

4. No Conclusion: In some cases, no consistent field star set could be found. Most often this was due to a relative paucity of field stars in the vicinity of the KBO, in combination with a large scatter in both the ellipse axis ratio and the axis angle among the stars available. Without a consistent field star group, the average star ellipse parameters with which to fit the KBO could not be determined. In

other cases, the KBO image was contaminated by a nearby field star, whose signal swamped that of the KBO itself.

Provisional Designation	R-mag	Date	Peak Ratio	PR Error	Row Offset	Row Error	Column Offset	Column Error	Conclusion
2001 KX76	19.0	2001.05.31	0.01	0.006	-1.72	0.6	0.41	0.4	Possible No Conclusion
2000 QC243	19.5	2000.08.26	``	``	``	``	``	``	Circular
2001 QY297	20.3	2001.08.20	1.147 0.10	0.80 0.06	-1.12 -1.78	0.13 0.6	0.18 -0.69	0.18 0.45	Candidate Possible
2000 QB243	20.4	2000.08.24	0.4	0.9	0.7	0.5	0.8	0.5	Possible
2001 KD77	20.5	2001.05.23	33	14	-2.55	0.5	0.88	0.5	Circular
2000 OK67	21.2	2000.07.28	``	``	``	``	``	``	No Conclusion
2001 KA77	21.2	2001.05.23	``	``	``	``	``	``	Circular
2000 CN105	21.4	2000.02.06	0.06	0.02	-2.69	0.5	-2.52	0.5	Possible
2001 KC77	21.5	2001.05.22	0.074 0.39	0.04 0.08	-1.90 -0.92	0.6 0.15	1.05 1.56	0.6 0.16	Possible Candidate

Table 6.1. Dual-source parameter values for a subset of the candidate Kuiper Belt Objects tested. The peak ratio and the row and column offsets of a possible companion body are given, with their standard errors. `` indicates that no number was available for that parameter. For a complete list of results with explanatory notes, see Appendix B.

Four of the KBOs tested were classified as candidate binary objects. One of these, 2001 QT297, is a known binary. Also, twelve were classified as possible binary candidates, while twenty-two were determined to be circular within detection limits, and no conclusion could be reached for the remaining seven objects. Because of the increasing error in the ellipse parameters with the progression to fainter R-magnitudes, the method reaches its detection limits between R=22.3 mag and R=22.5 mag.

6.3 Detection Limits

To test the resolution of dual-source elliptical fitting, I created synthetic data for several binary systems with different peak ratios and component separations. Representative values for the ellipse parameters (diameter, 2.2 pixels; shape index, 3.6; axis angle, 30 degrees; axis ratio, 0.90) were prescribed from my experience with fitting Mosaic images. To simulate real data, Gaussian noise was added to each of the synthetic binary images, with mean zero and standard deviation of one.

By looking at the images, I estimated that a signal-to-noise (S/N) ratio of 15 for the brightest pixel corresponds to the S/N ratio of an approximately 22.0 magnitude KBO Mosaic image. The detection limits of this method for a S/N ratio of 15 are given in Figure 6.1 below. I also asked two other students in the department to choose those images from among the data set that they

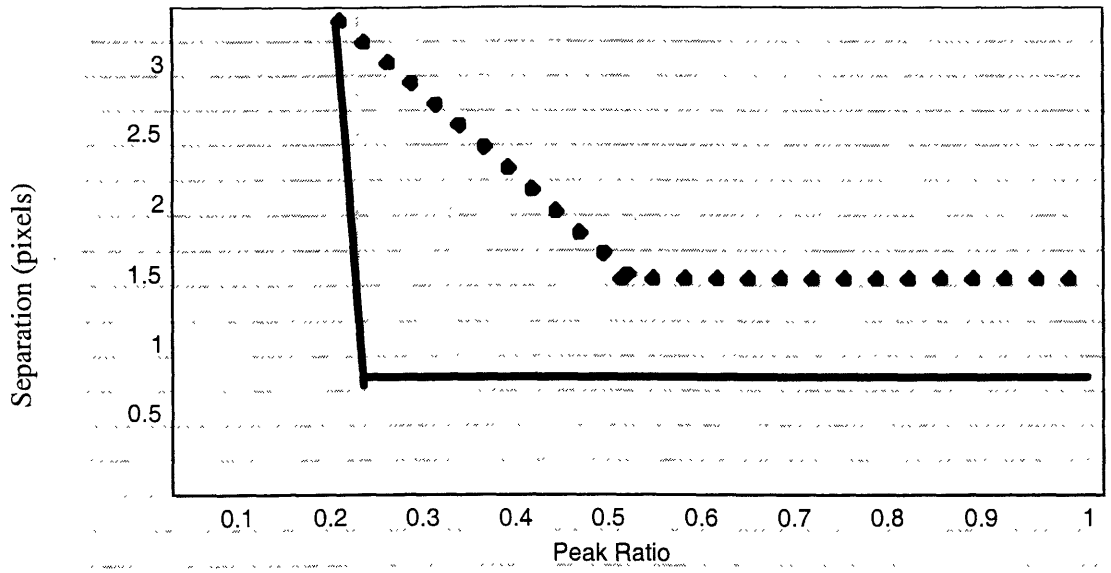

Figure 6.1. Detection Limits for a signal-to-noise ratio of 15. The dotted line indicates the approximate limit of visual dection, and the solid line the detection limit of the fitting technique. The horizontal lines indicate the limits of spatial resolution; the vertical lines, the brightness of the secondary KBO component. I noticed that the fitting, when it converged, sometimes tended to overestimate the actual peak ratio and separation distance.

would identify visually as binary, and from our three opinions the visual detection limit is plotted on the same.

Below the solid horizontal line, the dual-source fit collapsed into a single source. The position of the line corresponds to the angular resolution of the telescope: as the resolution is increased, the detection limit will be lowered.

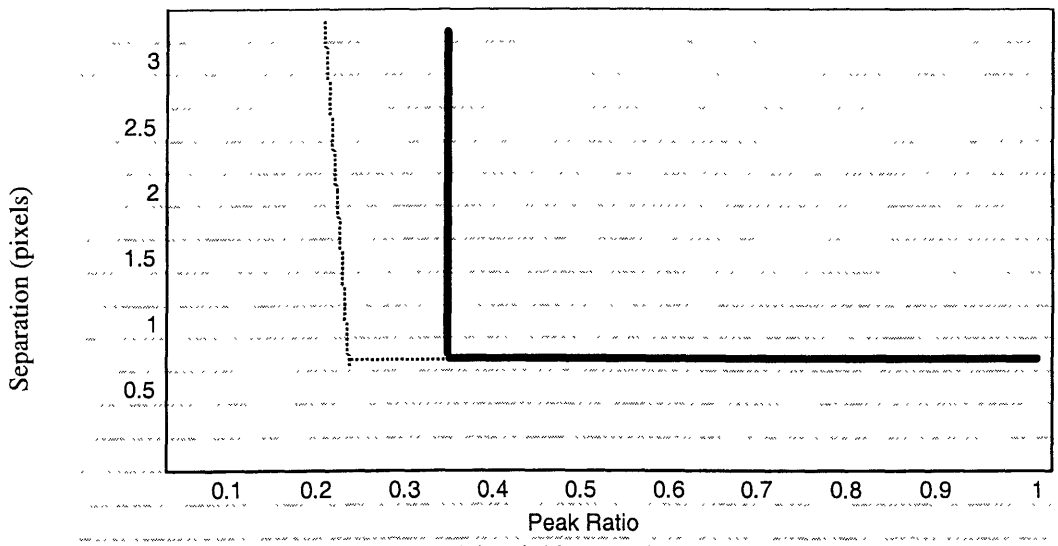

Figure 6.2 Detection limits for a S/N ratio of 5 (solid line) and 15 (dotted line, same as in 6.1).

The nearly vertical resolution limit is a function of the frame's signal-to-noise ratio. For a given S/N ratio, there is a peak ratio such that the brightness of the secondary component is comparable to the magnitude of the noise, and cannot be differentiated from it. The reduced binary detection range as the signal becomes fainter is illustrated in Figure 6.2.

An interesting side note is that among the synthetic binary data I included the images of the KBOs 2001KH76 and 2001KC77. The latter object, which is on my candidate binary list, was picked out as one of the likely binary objects by both unbiased observers (unbiased meaning not me); 2001KH76, which is not on my list, was not selected.

Chapter 7. Magellan Observations

7.1 Spring 2002 Observing Runs

High precision photometry observations of the ten candidate binary KBO systems on the priority list and visible during April were attempted with the Magellan telescopes at the Las Campanas Observatory in Chile, during the nights of April 8-11, 2002.

The target list for Magellan observations is comprised of (1) those DES image objects that are strong candidates, showing a good dual-source fit, and (2) DES image objects with small but nonzero calculated peak ratios: PR ≈ 0.10. The orbital parameters for each of these objects during the time of April observation are given in Table 7.1.

Object Name	**RA (J2000)**	**DEC (J2000)**	**R**	**Error(")**	**Rate("/hr)**
Candidates					
2001KC77*	15:58:23.531	-21:10:28.51	22.2	675.78	1.96
2001KK76*	16:33:58.307	-21:22:10.06	22.0	162.90	1.33
Possible Candidates					
2000CQ105	09:20:06.161	+18:15:20.00	22.7	0.15	1.31
2000CM105	09:20:35.424	+19:30:45.22	22.2	0.16	1.49
2001QB298*	21:54:50.122	-11:38:13.20	22.0	1732.02	3.21
28978	16:23:35.406	-19:54:15.51	19.4	0.21	1.50
2000CN105	10:14:53.502	+13:59:21.46	21.4	0.16	1.99
2001KJ76*	16:04:40.264	-22:36:30.23	22.6	1723.07	1.65
2000CN114	09:29:21.796	+16:14:29.00	23.5	0.31	1.56
2001KU76*	14:29:47.107	-13:32:34.35	22.1	99.48	2.83

Table 7.1. KBO Positions for April 2002 for the objects on the Magellan target list. Starred objects required updated positions from recovery during the DES run at CTIO immediately preceding the Magellan run in order to be observed with Magellan; the positional error for the latter should be limited to less than 30".

The goal for Magellan observations is to increase the S/N ratio to at least five times that of the corresponding DES images.

The integration time for each frame is limited by the rate of motion of the KBO: the distance traveled should be less than 0".1. The maximum allowable integration time is therefore

$$T(\text{sec}) = \frac{0".1}{v("/hr)} * 3600 \qquad (8)$$

or, for example, 184 seconds (~3 min) for 2001KC297, which was moving at approximately 1.96"/hr in April 2002.

The number of frames taken therefore will be proportional to the diameter of the objects on the frame, or inversely to the seeing, such that the required S/N ratio is attained:

$$\frac{\left(\frac{S}{N}\right)_{\text{Magellan}}}{\left(\frac{S}{N}\right)_{\text{DES}}} = \frac{6.5\text{m}}{4\text{m}} * \frac{D_{\text{DES}}}{D_{\text{Magellan}}} * \sqrt{\frac{T_{\text{Magellan}}}{T_{\text{DES}}}} * \sqrt{\frac{F_{\text{Magellan}}}{F_{\text{DES}}}} \quad (9)$$

where D_{DES} and D_{Magellan} are the image diameters in the Mosaic and Magellan frames, respectively, T_{DES} and T_{Magellan} are the respective frame integration times, and F_{Magellan} and F_{DES} are the number of frames taken. T_{DES} is fixed, and the maximum value of T_{Magellan} is constrained by Equation (8).

Unfortunately, no good observations could be obtained during the nights of the observing run, due to cloudy conditions and 100% relative humidity requiring that the telescope be shut down. This began partway through the night of April 8-9, and the high humidity lasted throughout the next few days.

Observations will continue to be attempted; the next observing run at Magellan is during the first week of July. The following table lists the approximate positions of the visible candidate binaries during that time frame.

Object Name	**RA (J2000)**	**DEC (J2000)**	**R-magnitude**
Candidates			
2001 QY297	20:51:05.76	–18:13:05.8	20.3
2001KC77	15:53:30.64	–21:00:40.1	21.5
2001KK76	16:29:56.91	–21:13:45.9	21.9
Possible Candidates			
2000 QB243	21:40:33.42	–15:16:45.4	20.4
2000 OJ67	21:47:05.72	–14:13:22.0	21.6
28978	16:19:28.91	–19:47:26.5	19.4
2001QX297	22:06:28.56	–10:54:24.9	22.1
2000OO67	23:00:23.81	–12:43:05.4	22.2
2001KU76	14:25:19.95	–13:13:51.8	22.1

Table 7.2. KBO Positions for June 2002 for the objects on the Magellan target list. The objects 2001KC77, 2001KK76 and 2001KU76 were recovered by the DES in April, reducing their errors; the objects 2001QB298 and 2001KJ76 were not and are removed from the June observing list.

7.2 Archival Image Frames

Flat-fielded image frames were available in the database for the objects 2000CM105 and 2000CN105. Both these objects were categorized as "possible" binaries because they had small (but nonzero within 1σ error bars) fitted peak ratios; they will not be observable during the June observing run.

These images were tested using the procedure detailed earlier, with small modifications due to the different nature of the images: the extracted portion of the image file was increased to

500x500 pixels, and the extracted box size for each stellar and KBO image to 30x30 pixels, to accommodate the increased image diameter and plate scale. The results are presented in Table 7.2 below, which compares the Magellan results to the conclusions made on the basis of the Mosaic frames.

Object	Source	Frame	Peak ratio	±	Row offset (pixels)	±	Column offset (pixels)	±	Conclusions
2000 CM105	DES	000206.007	0.10	0.04	-1.69	0.4	0.65	0.4	Possible
	DES	000206.035	``	``	``	``	``	``	No Conclusion
	Magellan	020212.102	-0.07	0.03	4.0	1.0	-0.9	0.8	Circular
2000 CN105	DES	000206.018	0.06	0.02	-2.69	0.5	-2.52	0.5	Possible
	DES	000206.047	``	``	``	``	``	``	No Conclusion
	Magellan	020212.126	-0.04	0.02	-7.5	0.7	1.1	0.6	Circular

Table 7.3 Fitting results of the Mosaic and Magellan images for the two KBOs for which Magellan archival images exist. The plate scale is 0".526/pixel for the Mosaic and 0". for the Magellan images. The "No Conclusion" in the DES data frames is a consequence of the absence of a consistent star set.

Neither Kuiper Belt Object showed binarity in its Magellan frame; the peak ratio converged to a slightly negative value both times. This indicates that the small peak ratio obtained in the DES image data was likely a function of noise. These findings were not unexpected, since a peak ratio of 0.10 is at or beyond the detection limits of this method (see Section 6.3) for R-magnitudes of 22.2 (2000CM105) and 21.4 (2000CN105).

Chapter 8. Conclusions

8.1 Synopsis

A method has been developed, as shown in Chapter 5, for examining archival image frames containing Kuiper Belt objects and partitioning those KBOs into binary candidate / not binary classifications. This method relies on the fact that a binary KBO system will appear in a telescope image as an elongated source, with more or less elongation depending on the separation distance and the relative luminosity of the two components.

Using this method, Mosaic images for forty-five Kuiper Belt objects were tested to determine their candidacy as binary objects. Of these, four were candidate binary, twelve others were possible candidates, twenty-one were circular within detection limits, and seven lacked the consistent set of field stars necessary for determination.

Due to unfavorable observing conditions during the three nights of the run, no good images of the ten candidate binaries and possible candidates visible during the April 2002 observing run were able to be taken with the Magellan telescope. Another attempt will be made this June.

Archival Magellan images of 2000CM105 and 2000CN105 were examined. Originally classified as "possible" candidates due to their fitted peak ratios greater than zero but less than 0.10, they did not show duplicity in the Magellan frames.

8.2 Future Research

This methodology of image analysis should continue to be applied, as the Deep Ecliptic Survey continues in its discovery of Kuiper Belt objects, to examine the detection images and classify additional binary candidates.

The testing process has been adapted for application to images taken with the Magellan telescopes. Future work should include image analysis for archival and new Magellan KBO frames, with an expectation of better resolution and lower detection limits. The candidates selected as a result of this thesis work may be imaged during a future Magellan observing run. The method could also be easily adapted to data from other telescope image frames.

For those KBOs determined to be binary, further observations should be made over time to establish their mutual orbits. Observation of mutual events is highly encouraged during such time as the companions undergo occultations and eclipses visible from Earth.

References

Allen, R.L., Bernstein, G.M., & Malhotra, R., 2001, *ApJ*, 549, L241.

Barucci, M.A., Romon, J., Doressoundiram, A., & Tholen, D.J., 2000, *AJ*, 120, 496.

Barucci, M.A., Fulchignoni, M., Birlan, M., et al., 2001, *A&A*, 371, 1150.

Binzel & Hubbard, 1998, Pluto and Charon., eds. S. Alan Stern & David J. Tholen (University of Arizona Press), 85.

Bosh, A. S., L. A. Young, J. L. Elliot, H. B. Hammel, and R. L. Baron 1992, *Icarus* 95, 319-324.

Brown, M.E., Blake, G.A., & Kessler, J.E., 2000, *ApJ*, 543, L163.

Brown, M.E. 2001, *AJ*, 121, 2804.

Brown, M.E. submitted to *ApJL*.

Chiang, E.I., & Brown, M.E., 1999, *AJ*, 118, 1411.

Cruikshank, D.P., Roush, T.L., Bartholomew, M.J., et al., 1998, *Icarus*, 135, 389.

Davies, J.K., Green, S., McBride, N., Muzzerall, E., Tholen, D.J., Whiteley, R.J., Foster, M.J., & Hillier, J.K., 2000, *Icarus*, 146, 253.

Davis, D.R., & Farinella, P., 1997, *Icarus*, 125, 50.

Delsanti, A.C., Boehnhardt, H., Barrera, L., Meech, K.J., Sekiguchi, T., & Hainaut, O.R., 2001, *A&A*, 380, 347.

DeSanctis, M.C., Capria, M.T., & Coradini, A., 2001, *AJ*, 121, 2792.

Dones, L., 1997, in ASP Conf. Ser. 122, From Stardust to Planetesimals, ed. Y.J. Pendleton & A.G.G.M. Tielens (San Francisco: ASP), 347.

Duncan, M.J., Levison, H.F., & Budd, S.M., 1995, *AJ*, 110, 3073.

Duncan, M., Quinn, T., & Tremaine, S., 1988, *ApJ*, 328, L69.

Durda D.D., & Stern S.A. 2000, *Icarus*, 145, 220.

Edgeworth, K.E., 1943, *J. British Astron. Assoc.*, 53, 181.

Elliot, J.L., Kern, S.D., Millis, R.L., Buie, M.W., Wasserman, L.H., & Wagner, R.M. 2000, *Bulletin of the AAS*, 32, 3, 1029.

Elliot, J.L., Dunham, E.W., Bosh, A.S., Slivan, S.M., Young, L.A., Wasserman, L.H., & Millis, R.L. 1989, *Icarus*, 77, 148 .

Elliot, J.L., Dunham, E.W., Baron, R.L., Watts, A.W., Kruse, S.P., Rose, W.R., Gillespie, C.M., 1989b, *Pub. of the Astron. Soc. of the Pacific*, 101, 737.

Elliot, J.L., Kern, S.D., Millis, R.L., Buie, M.W., Wasserman, L.H., & Wagner, R.M., 2000, *BAAS*, 32, Div. Planet. Sci. abstr. No. 20.02.

Elliot, J.L, 2001, *IAU Circular* 7733.

Farinella, P., & Davis, D., 1996, *Science*, 273, 938.

Ferrin, I., et al., 2001, *ApJ*, 548, L243.

Fernandez, J.A., 1980, *MNRAS*, 192, 481.

Gladman, B., Kavelaars, J.J., Nicholson, P.D., Loredo, T.J., & Burns, J.A., 1998, *AJ*, 116, 2042.

Gladman, B., Kavelaars, J.J., Petit, J.-M., Morbidelli, A., Holman, M.J., & Loredo, T., 2001, *AJ*, 116, 2042.

Green, S.F., McBride, N., O'Ceallaigh, D., Fitzsimmons, A., Williams, I., & Irwin, M., 1997, *MNRAS*, 290, 186.

Hahn, J.M., & Malhotra, R., 1999, *AJ*, 117, 3041.

Hahn, J.M., 2000, in Lunar and Planetary Science XXXI (Houston: Lunar Planet. Inst.), No. 1888.

Hahn, J.M., & Ward, W.R., 2002, in Lunar & Planetary Science XXIII (Houston: Lunar Planet. Inst.).
Hainaut, O.R., & Delsanti, A.C., 2001, *A&A*, submitted.
Ida, S., Bryden, G., Lin, D.N.C., & Tanaka, H., 2000a, *ApJ*, 534, 428.
Ida, S., Larwood, J., & Burkert, A., 2000b, *ApJ*, 528, 351.
Jewitt, D.D., & Luu, J.X. 1993, *Nature*, 362, 730.
Jewitt, D., Luu, J., & Chen, J., 1996, *AJ*, 112, 1225.
Jewitt, D., Luu, J., & Trujillo, C., 1998, *AJ*, 115, 2125.
Jewitt, D., & Luu, J., 1998, *AJ*, 115, 1667.
Jewitt, D., Luu, J., & Trujillo, C., 1998, *AJ*, 115, 2125.
Jewitt, D.C., & Luu, J.X., 2000, in Protostars and Planets IV, ed. V. Mannings, A.P. Boss, & S.S. Russell (Tucson: Univ. AZ Press), 1201.
Jewitt, D.C., & Luu, J.X., 2001, *AJ*, 122, 2099.
Jewitt, D.C., & Luu, J.X., 1993, *Nature*, 362, 730.
Jewitt, D., 2002, *AJ*, 123, 1039.
Kavelaars, J., Gladman, B., Petit, J.-M., Holman, M., 2001, *IAU Circular* 7749.
Kenyon, S.J., & Windhorst, R.A., 2001, *ApJ*, 547, 69.
Kuiper, G.P., 1951, On the Origin of the Solar System, ed. J.A. Hynek (New York: McGraw-Hill), 357.
Larsen, J.A., et al., 2001, *AJ*, 115, 2125.
Levison, H.F., Lissauer, J.J., & Duncan, M.J., 1998, *AJ*, 116, 1998.
Levison, H.F., & Stern, S.A., 2001, *AJ*, 121, 1730.
Luu, J., & Jewitt, D., 1996, *AJ*, 112, 2310.
Luu, J., & Jewitt, D., 1998, *ApJ*, 502, L91.
Malhotra, R., 1995, *AJ*, 110, 420.
Millis, R.L., Buie, M.W., Wasserman, L.H., Elliot, J.L., Kern, S.D., Wagner, R.M., 2000, *BAAS*, 32, 1028.
Millis, R.L., Buie, M.W., Wasserman, L.H., Elliot, J.L., Kern, S.D., Wagner, R.M., 2002, *AJ*, 123, 2083.
Morbidelli, A., & Valsecchi, G.B., 1997, *Icarus*, 141, 367.
Nagasawa, Tanaka, & Ida, 2000, *AJ*, 120, 3311.
Noll, K., & Stephens, D., et al., 2002, *IAU Circulars* 7824, 7857.
Petit, J.-M., Morbidelli, A., & Valsecchi, G.B., 1999, *Icarus*, 141, 367.
Sheppard, S.S., Jewitt, D.C., Trujillo, C.A., Brown M.J.I., & Ashley, M.C.B.A., 2000, *AJ*, 120, 2687.
Stephens, J.R., & Gustafson, B.A.S., 1991, *Icarus*, 94, 209.
Stern, S.A., & Colwell, J.E., 1997, *ApJ*, 490, 879.
Tegler, S.C., & Romanishin, W., 1998, *Nature*, 392, 49.
Tegler, S.C., & Romanishin, W., 2000, *Nature*, 407, 979.
Trujillo, C.A., Jewitt, D.C., & Luu, J.X., 2001, *AJ*, 122, 457.
Trujillo, C.A., Luu, J.X., Bosh, A.S., & Elliot, J.L., 2001, *AJ*, 122, 2740.
Trujillo, C.A., & Brown, M.E., 2001, *ApJ*, 554, L95.
Trujillo, C.A., Jewitt, D.C., & Luu, J.X., 2001, *AJ*, 122, 457 (01TJL).
Trujillo, C.A., & Brown, M.E., 2002, *ApJ*, 566, L125.
Trujillo, C.A., & Brown, M.E., 2002, *IAU Circulars* 7787, 7807.

Veillet, C. 2001, *IAU Circular* 7610.
Wilson, P.D., Sagan, C., & Thompson, W.R., 1994, *Icarus*, 107, 288.

Appendix A – Image Analysis Frames

Sample Extraction Image

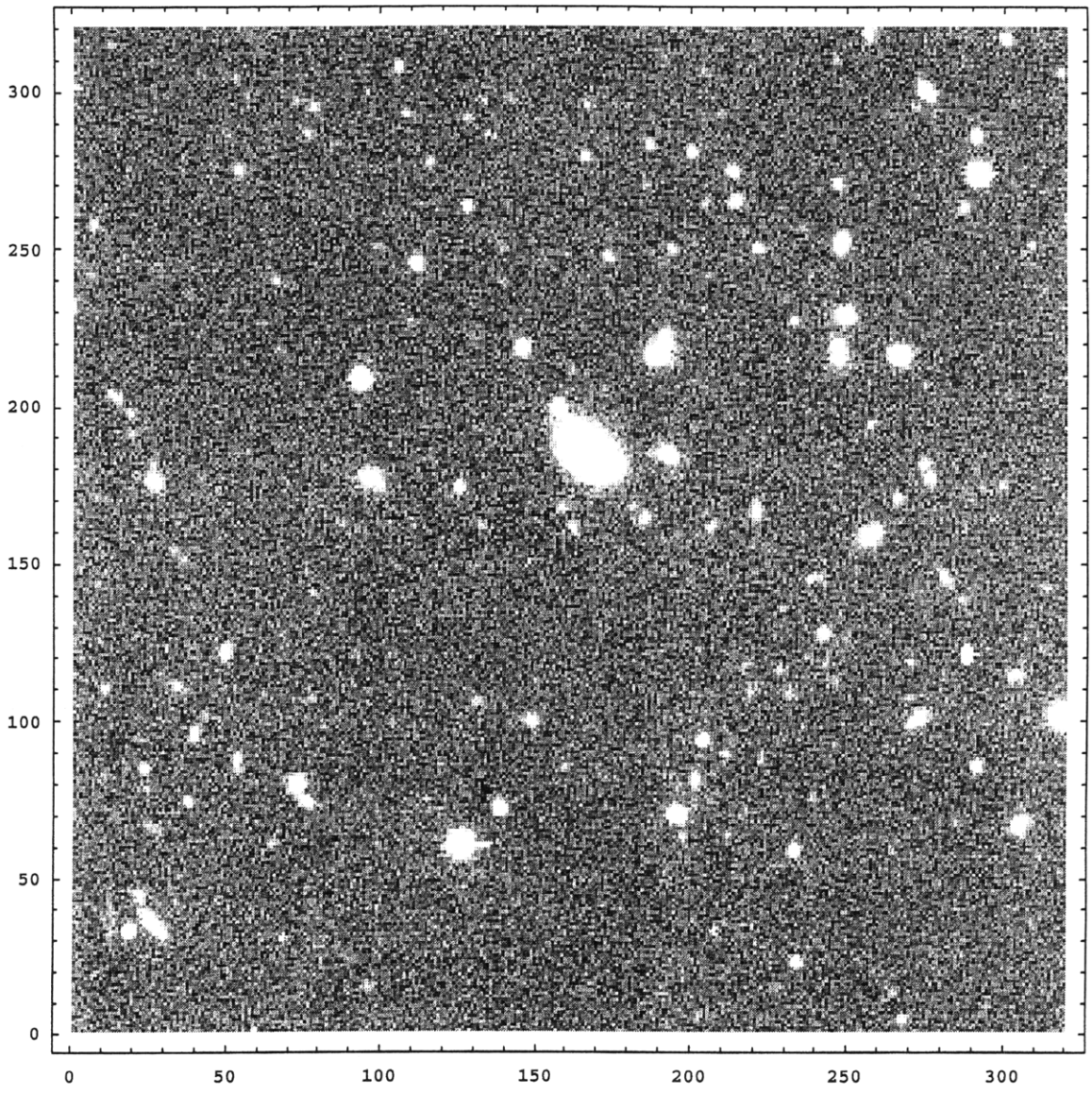

The KBO QT297 is located at {161, 162}.
Extraction from the file *20000731.096.fits*

Plot of a "Good" Set of Residuals

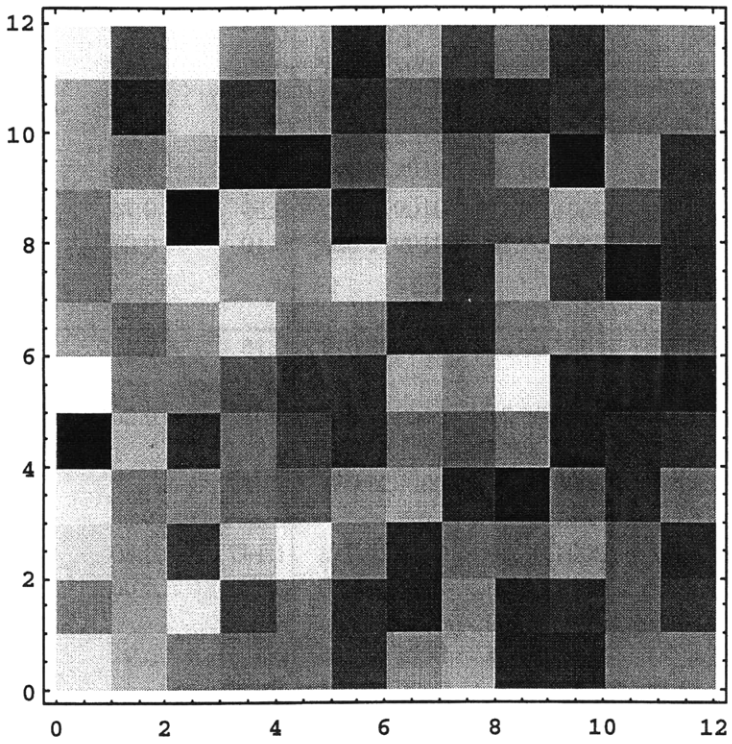

Plot of a "Bad" Set of Residuals (presumably a galaxy)

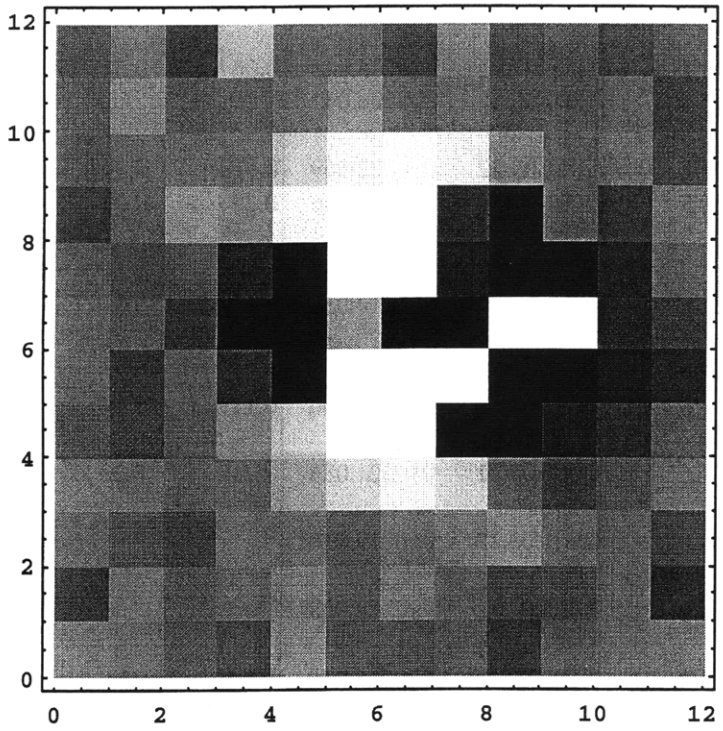

Appendix B - Table of Fitting Results

Local Designation	Provisional Desig.	Magnitude	Date	Image Frame	Peak Ratio	PR Error
	2001 QT297	21.0	2000.07.31	000731.096	0.62	0.17
	2001 QT297	21.0	2000.07.31	000731.077	0.67	0.17
	2001 QT297	21.0	2001.08.19	010819.019	``	``
	2001 QT297	21.0	2001.08.20	010820.039	1.76	0.8
	2001 QT297	21.0	2001.08.20	010820.057	0.65	1.1
	2001 QT297	21.0	2001.09.12	010912.015	0.59	0.76
	2001 QT297	21.0	2001.09.12	010912.028	0.10	0.08
"new KBO"	2002CY224	21.1	2002.02.08	020208.019	0.15	0.45
MB27454	2001 KX76	19.0	2001.05.21	010521.080	0.01	0.006
MB17597	2000 QC243	19.5	2000.08.26	000826.031	``	``
MB37344	2001 QY297	20.3	2001.08.20	010820.032	1.147	0.80
MB37344	2001 QY297	20.3	2001.08.20	010820.050	0.10	0.06
MB12992	2000 QB243	20.4	2000.08.24	000824.015	0.4	0.9
MB32735	2001 KD77	20.5	2001.05.23	010523.077	33	14
MB7007	2000 OK67	21.2	2000.07.28	000728.080	``	``
MB32600	2001 KA77	21.2	2001.05.23	010523.075	``	``
MB2199	2000 CN105	21.4	2000.02.06	000206.018	0.06	0.02
MB2199	2000 CN105	21.4	2000.02.06	000206.047	``	``
MB29896	2001 KC77	21.5	2001.05.22	010522.069	0.074	0.04
MB29896	2001 KC77	21.5	2001.05.22	010522.086	0.39	0.08
MB36134	2001 QB298	21.5	2001.08.19	010819.039	0.48	1.5
MB36134	2001 QB298	21.5	2001.08.19	010819.058	0.22	0.5
MB7008	2000 OJ67	21.6	2000.07.28	000728.072	0.21	0.25
MB7008	2000 OJ67	21.6	2000.07.28	000728.100	0.11	0.10
MB27980	2001 KY76	21.6	2001.05.21	010521.089	-0.41	0.22
MB35934	2001 QR297	21.6	2001.08.19	010819.036	``	``
MB1996	1999 HB12	21.9	1999.04.18	990418.008	``	``
MB2200	2000 CJ105	21.9	2000.02.05	000205.070	0.34	24
MB2202	2000 CQ105	21.9	2000.02.05	000205.020	0.24	0.4
MB2202	2000 CQ105	21.9	2000.02.05	000205.044	0.15	0.07

Appendix B - Table of Fitting Results

Row Offset	Row Error	Column Offset	Column Error	Diameter	Conclusion	Notes*
-1.71	0.2	0.98	0.2	2.0	Binary	
-1.66	0.2	1.00	0.2	2.1	Binary	1
``	``	``	``	3.4		3
-0.98	0.2	1.29	0.2	2.4	Binary	
-0.77	0.4	0.75	0.3	2.5	Probably Binary	1
0.93	0.3	-0.74	0.4	2.5	Possible	2
-2.01	0.5	0.44	0.6	2.8	Binary	
0.69	0.9	0.68	0.9	2.5	Circular	
-1.72	0.6	0.41	0.4	1.9	Possible	4, 6
``	``	``	``	1.9	Circular	3
-1.12	0.13	0.18	0.18	2.4	Candidate	
-1.78	0.6	-0.69	0.45	2.4		2
0.7	0.5	0.8	0.5	3.7	Possible	4, 6
-2.55	0.5	0.88	0.5	2.0	Circular	
``	``	``	``	``	``	7
``	``	``	``	2.1	Circular	3
-2.69	0.5	-2.52	0.5	2.1	Possible (Faint)	
``	``	``	``	``	``	7
-1.90	0.6	1.05	0.6	2.3	Possible (Faint)	4
-0.92	0.15	1.56	0.16	2.1	Candidate	
-1.59	1.2	-0.76	1.1	4.0	Possible	4,8
6.18	3.8	-5.14	1.8	3.4		8
-0.54	0.41	0.99	0.58	2.1	Possible	4
-0.75	0.56	-1.19	0.68	1.9	Possible	2
-3.87	0.7	2.45	0.7	2.0	Circular	10
``	``	``	``	4.5	Circular	3
``	``	``	``	3.8	Circular	3
-0.16	3	-0.15	3	1.7	Not Candidate	8
-0.60	0.8	1.41	1.0	2.4	Possible	4,8
2.28	0.5	-0.48	0.48	1.9	Possible	9

Appendix B - Table of Fitting Results

Local Designation	Provisional Desig.	Magnitude	Date	Image Frame	Peak Ratio	PR Error
MB32265	2001 KK76	21.9	2001.05.23	010523.070	0.46	0.06
MB32265	2001 KK76	21.9	2001.05.23	010523.087	0.07	0.04
MB30090	2001 KP76	21.9	2001.05.22	010522.073	0.72	1.31
MB28994	2001 KB77	21.9	2001.05.22	010522.030	0.03	0.04
MB28994	2001 KB77	21.9	2001.05.22	010522.052	-0.3	1.5
MB35595	2001 QS297	21.9	2001.08.19	010819.037	``	``
MB35595	2001 QS297	21.9	2001.08.19	010819.056	``	``
MB2203	2000 CL104	22.0	2000.02.05	000205.063	``	``
MB2203	2000 CL104	22.0	2000.02.05	000205.086	0.04	0.05
MB2201	2000 CH105	22.0	2000.02.05	000205.069	0.14	0.3
MB2201	2000 CH105	22.0	2000.02.05	000205.092	``	``
MB7009	2000 OU69	22.0	2000.07.28	000728.031	``	``
MB27240	2001 KG76	22.0	2001.05.22	010522.076	0.40	5
MB27603	2001 KH76	22.0	2001.05.22	010521.083	``	``
MB2204	2000 CM105	22.1	2000.02.06	000206.007	0.10	0.04
MB2204	2000 CM105	22.1	2000.02.06	000206.035	``	``
MB8711	2000 OM67	22.1	2000.07.30	000730.085		
MB7015	2000 OO67	22.1	2000.07.28	000728.081	0.049	0.046
MB7015	2000 OO67	22.1	2000.07.28	000728.108	0.077	0.05
MB36156	2001 QU297	22.1	2001.08.19	010819.040	5	39
MB15250	2001 QW297	22.1	2000.08.25	000825.020	``	``
MB19400	2001 QX297	22.1	2000.08.27	000827.028	0.15	0.09
MB19400	2001 QX297	22.1	2000.08.27	000827.043	0.08	0.05
MB1995	1999 HS11	22.2	1999.04.17	990417.015	0.28	0.6
MB1995	1999 HS11	22.2	1999.04.17	990417.030	0.15	0.13
MB3380	2000 CN114	22.2	2000.02.05	000205.074	0.17	0.11
MB24638	2001 FP185	22.2	2001.03.26	010326.017	``	``
MB24638	2001 FP185	22.2	2001.03.26	010326.039	``	``
MB30076	2001 KJ76	22.2	2001.05.22	010522.072	0.13	0.06
MB30076	2001 KJ76	22.2	2001.05.22	010522.089	0.43	0.9

Appendix B - Table of Fitting Results

Row Offset	Row Error	Column Offset	Column Error	Diameter	Conclusion	Notes*
0.50	0.2	-2.27	0.13	2.1	Candidate	
-1.96	0.7	-1.58	0.7	1.9	Possible (Faint)	9
0.22	0.31	0.89	0.26	2.0	Circular	
5.44	2.7	-3.95	1.8	2.7	Circular	
0.4	2	0.4	1.8	2.3	Circular	
``	``	``	``	``	``	7
``	``	``	``	``	``	7
``	``	``	``	``	``	7
-1.96	1.5	-0.11	1.2	1.9	Circular	
0.62	0.55	0.60	0.62	1.5	Possible	4,8
``	``	``	``	``	``	7
``	``	``	``	``	``	7
-0.36	1	-0.33	1	2.1	Circular	8
``	``	``	``	2.1	Circular	3
-1.69	0.4	0.65	0.4	1.7	Possible	4
``	``	``	``	``	``	7
				``		6
-1.40	1.0	1.89	1.0	1.7	Possible (Faint)	4
-2.43	0.8	0.19	0.7	2.0	Possible (Faint)	4
-1.5	4.6	-0.14	2.8	3.0	Circular	
``	``	``	``	1.9	Circular	3
-1.41	0.7	-1.39	0.6	2.3	Possible	4
-2.06	1.0	-0.33	0.8	2.1	Possible	4,1
0.025	0.6	1.27	1.0	2.6	Possible	8
-1.28	0.9	-1.55	0.9	3.0	Most Likely Circula	8,9
-0.82	0.6	-1.43	0.6	1.9	Possible	
``	``	``	``	``	``	7
``	``	``	``	``	``	7
-1.34	0.6	1.75	0.6	2.0	Possible	
-0.94	0.6	-0.10	0.4	2.1	Possible	2,8

Appendix B - Table of Fitting Results

Local Designation	Provisional Desig.	Magnitude	Date	Image Frame	Peak Ratio	PR Error
MB31976	2001 KU76	22.2	2001.05.23	010523.037	0.21	0.10
MB31976	2001 KU76	22.2	2001.05.23	010523.064	0.12	0.15
MB7011	2001 QA298	22.2	2000.07.28	000728.062	0.12	0.08
MB39183	2001 QJ298	22.2	2001.08.20	010820.045	0.34	0.4
MB36185	2001 QV297	22.3	2001.08.19	010819.040	``	``
MB45702	(02CQ154)	22.4	2002.02.06	020206.067	0.17	0.09
MB45702	(02CQ154)	22.4	2002.02.06	020206.058	-0.05	2
MB45323	(02CP154)	22.0	2002.02.06	020206.035	0.34	0.07
MB45323	(02CP154)	22.0	2002.02.06	020206.058	-0.1	0.1
MB46433	(02CX154)	22.0	2002.02.06	020206.105	``	``
MB45312	(02CU154)	22.3	2002.02.06	020206.035	PR << 0	

*Notes:
1 - Consistent with paired frame
2 - Consistent except columns
3 - Double-source fit collapsed and/or blew up
4 - Peak Ratio is faint, or zero/one within error
5 - Image contaminated with overlapping star
6 - Frame(s) do not exist
7 - No Consistent Star Set
8 - Errors dominate
9 - Not consistent with paired frame
10 - Peak ratio became negative
11 - Second source attempted to fit a nearby star

Appendix B - Table of Fitting Results

Row Offset	Row Error	Column Offset	Column Error	Diameter	Conclusion	Notes*
-0.48	0.4	2.03	0.5	2.2	Possible	
-0.75	0.9	1.45	1.1	2.4	Possible	1
-1.27	0.7	-2.24	0.7	1.7	Possible / Circular	(3)
-6.1	0.6	-3.4	0.5	2.7	Circular	11
``	``	``	``	``	`` / Circular	4,7
-3.30	0.7	0.50	0.8	2.3	Circular	11
-0.16	68	0.10	27	2.1	Circular	3,8,10
2.00	0.2	0.37	0.2	2.0	No Conclusion	5
3.05	1.5	-0.91	1.5	2.8	Circular	10
``	``	``	``	``	``	7
				2.2	Circular	10